Published in final edited form as:
Adv Healthc Mater. 2012 January 11; 1(1): . doi:10.1002/adhm.201100005.

Cooperative, nanoparticle-enabled thermal therapy of breast cancer

Haifa Shen[1,3,4], **Jian You**[2,3], **Guodong Zhang**[1], **Arturas Ziemys**[1], **Qingpo Li**[1], **Litao Bai**[1], **Xiaoyong Deng**[1], **Donald R. Erm**[1], **Xuewu Liu**[1], **Chun Li**[2], and **Mauro Ferrari**[1,4]

[1]The Methodist Hospital Research Institute, Department of Nanomedicine, 6670 Bertner Ave., Houston, Texas 77030

[2]The University of Texas M D Anderson Cancer Center, Department of Experimental Diagnostic Imaging, 1515 Holcombe Blvd., Houston, Texas 77030

Keywords

gold; porous silicon; nanoassembly; thermal therapy

Despite decades of effort on research and drug development for cancer treatment, cancer still remains one of the major causes of human deaths in the world [1]. Human cancers consist of mixed population of malignant cells that carry multiple genetic mutations. It has been estimated that there are around 40 DNA mutations that result in amino acid changes in an individual tumor of glioblastoma [2] or pancreatic cancer [3], and twice as many mutations in breast and colorectal cancers [4]. Many of them are driver mutations that determine tumor initiation, progression and metastasis. The genomic landscapes indicate that multiple signal transduction pathways determine the fate of a cancer cell, and it is almost impossible to treat cancer with a single therapeutic agent. It is thus not surprising that many of the recently developed targeted therapy drugs, such as the EGFR inhibitors for non-small-cell lung cancer treatment and Herceptin for breast cancer therapy, are effective in only a certain set of cancer patients [5, 6]; and in many cases, drug resistance arises from additional genetic and epigenetic alterations. It has been reported that mutations within the EGFR gene [7, 8], the KRAS gene [9, 10], and up-regulation of other signaling pathways [11, 12] could all cause resistance to EGFR-targeted therapy. Clearly, there is an urgent and persistent motivation to develop novel therapeutics independent of cancer genetic background in the fight against this deadly disease.

Nanotechnology has played a crucial role in the development of cancer therapeutics[13]. Doxil™ and Abraxane™ [14–17] are just two examples of nanoformulated drugs. Gold nanoparticles are currently being explored to induce hyperthermic cytotoxicity [18–22]. When exposed to light at the right wavelength, the conduction-band electrons of the nanoparticle generate heat that is transmitted to the cells and surrounding tissues. Thermal therapy has the advantage of killing cancer cells without causing resistance regardless of genetic background, and thus can be applied to all cancer patients. However, successful application of this approach requires adequate accumulation of gold nanoparticles in the tumor and sufficient tumor penetration of the excitation energy [23]. Due to lack of effective delivery, tumor delivery of gold nanoparticles in most studies has been relied on the enhanced

[4]Corresponding Authors: Haifa Shen, The Methodist Hospital Research Institute, 6670 Bertner Ave., Houston, Texas 77030, hshen@tmhs.org. Mauro Ferrari, The Methodist Hospital Research Institute, 6670 Bertner Ave., Houston, Texas 77030, mferrari@tmhs.org.
[3]H.S. and J.Y. contributed equally to this work.

permeability and retention (EPR) effect, a result of tumor blood vessel leakiness due to a state of ongoing angiogenesis, and thus are not very efficient [24]. It has been reported that less than 5% of total injected dose of PEGylated gold nanoparticles could ultimately reach the tumor tissue [22]. The amount of gold nanoparticles needed for each treatment makes it impractical for clinic therapies. Besides, gold nanoparticles tend to accumulate unevenly in the tumor tissue dependent on particle size, surface charge, and other factors [25–27], which makes it difficult to eradicate the whole tumor tissue with this approach.

We have previously developed a multistage vector delivery system based on porous silicon (pSi). This system is comprised of two delivery carriers: the 1st stage biodegradable pSi vector and the 2nd stage nanoparticles loaded into the pores of pSi. The nanoparticles can be liposomes or micelles incorporated with therapeutics (the 3rd stage) or diagnostic agents [28]. A major advantage of this system is that the size, shape, and surface properties of pSi can be tailored so that maximal tissue-specific localization and release of the therapeutics at the target tumor can be achieved [28–31]. We have recently demonstrated successful application of this system to deliver siRNA therapeutics for cancer treatment with two mouse models of ovarian cancers [32, 33].

Here we designed pSi nanoassembly with hollow gold nanoshells (HAuNS) to explore photothermal effects for therapeutics taking advantage of the nanoscale effect. HAuNS are favorable over the solid gold nanoparticle (AuNP), since the near infrared (NIR) light for hollow gold has a deep penetration inside the body and causes less damage to tissues due to less absorbance by the tissue chromophores. We used human and mouse breast cancer lines to test cell killing *in vitro* and the mouse model of 4T1 mammary tumor for *in vivo* studies. The potential mechanism of action with the new therapeutics will be discussed.

pSi particles were fabricated over three major steps: formation of porous silicon films, photolithographic patterning of particles and reactive ion etch. The porous structure of particles was tailored by electrochemical etching to a mean pore size of 60 nm and a porosity of about 80%, while the particle sizes were precisely defined by photolithography to 1000 nm in diameter and 400 nm in thickness. Scanning electron microscope (SEM) images revealed that the pores were evenly distributed across the whole area (Fig. 1A & 1B). Since the surface of the silicon particles were conjugated with APTES, these particles were positively charged, which facilitated loading of the negatively-charged HAuNS by favorable electrostatic interactions (Fig. 1C). Multiple HAuNS particles could be found in each pore across the whole silicon microparticle.

We carried out spectrum scan to determine absorption profiles. The HAuNS particles with 28 nm in diameter showed a plasma resonance peak at 750 nm (Fig. 1D) that is observed for most of the HAuNS particles of similar size [34, 35]. This peak disappeared when the HAuNS particles were loaded into pSi. There was a small peak around 950 nm indicating a red shift of absorbance from pSi/HAuNS (Fig. 1D), while empty pSi particles did not have any significant absorption in the 400–1100 nm range. We have also measured absorption spectra of solid gold nanoparticles (AuNP) with a plasma resonance peak at 528 nm (Supplementary Fig. 1). Loading of AuNP into pSi also resulted in disappearance of the peak and a red shift of the small peak in the 600–750 nm range. Simple mix of AuNP with silicon did not result in disappearance of the plasma resonance peak (data not shown). The most plausible explanation for vanishing absorption from the pSi/HAuNS nanoassembly is a scattering effect from the pSi microparticle.

Water suspension of the particles was used to measure heat generation triggered by a NIR laser. pSi particle alone did not show any heat generation as expected and stayed at room temperature all the time with the NIR laser continuously on (Fig. 2). The temperature in the

HAuNS colloidal suspension increased by 10.9 °C and reached a steady level of 34.7 °C within 10 min. A bigger increase in temperature was observed in the pSi/HAuNS suspension. Temperature reached 45.0 °C within 7 min with almost twice as high temperature as with the same amount of colloidal HAuNS. There was an overall increase of 20.6 °C from the room temperature. Time constants for heat generation kinetics were calculated at 3.1 s for HAuNS and 1.9 s for pSi/HAuNS.

To test whether the enhanced thermal generation could be translated into efficient cell killing, we treated cancer cells with free HAuNS or pSi/HAuNS, and monitored cell growth by the MTT assay. pSi and AuNP were used as controls. The AuNP particles were not expected to have any effect on thermal cytotoxicity, as the NIR laser used in the study with a wavelength of 808 nm did not have any impact on the solid gold. We loaded different amount of HAuNS into a fixed number of silicon particles (2×10^9 HAuNS or 2×10^{10} HAuNS in 1×10^8 pSi), so that any changes in cell growth would be from the impact of HAuNS, but not silicon particles. As expected, neither free HAuNS nor pSi/HAuNS had any significant impact on cell growth when there was not enough HAuNS for heat generation (Fig. 3A). However, when the number of gold particles increased, the pSi/HAuNS was very efficient in killing cancer cells, while the effect from free HAuNS was mild (Fig. 3A). Further increase of HAuNS particle numbers resulted in cell killing from both free gold and the gold-silicon nanoassembly (data not shown). Similar trend was observed with the MDA-MB-231 and SK-BR-3 human breast cancer cells (Fig. 3A, upper and middle panels) and 4T1 murine mammary tumor cells (Fig. 3A, bottom panel). These results indicate that the thermal ablation effect is general, since these cell lines carry significant genetic background and diverse mutation spectra. For example, the SK-BR-3 cells overexpress the HER2 gene, while MDA-MB-231 is a triple-negative cell line lacking the expression of estrogen receptor, progesterone receptor, and HER2.

We used two dyes to detect cell viability after exposure to NIR laser. The nonfluorescent calcein AM was converted to the intensely green fluorescent calcein in live cells. Ethidum homodimer-1 (EthD-1) entered dead/dying cells through damaged membranes and bound to nucleic acid, producing a bright red fluorescence. Cells were treated with a low dose (1X, 6.25×10^9 HAuNS/well) and a high dose (4X, 2.5×10^{10} HAuNS/well) free HAuNS or pSi/HAuNS. Around 20% cells were positive for EthD-1 staining without NIR laser treatment (Supplementary Fig. 2). The free HAuNS-treated cells did not undergo significant cell death at the 1X dose (Fig. 3B, upper left). The amount of EthD-1-positive cells doubled with the 4X HAuNS dose (Fig. 3B, upper right); however, the percentage of dead cells was not as high as in the sample treated with the 1X dose pSi/HAuNS (Fig. 3B, upper right vs. bottom left). Up to 88% cancer cells treated with 4 x pSi/HAuNS were EthD-1-positive 24 hours after NIR treatment, comparing to less than 35% EthD-1-positive cells treated with 4 x HAuNS (Fig. 3B, bottom right). Quantitative analysis of cell death from these treatments is shown in Fig. 3C. This result was in perfect match with the thermal generation result that showed the increase of temperature was 3 times as fast from the same amount of HAuNS in nanoassembly as from free HAuNS. These results indicate that enhanced cancer cell killing can be achieved through packaging gold nanoshells into pSi nanoassembly.

In a proof-of-principle study, we generated murine 4T1 tumor mice to test the efficacy of thermal ablation by pSi/HAuNS on tumor growth. When tumor sizes reached 150–200 cm^3, free HAuNS or pSi/HAuNS were delivered by intra-tumor injection. The tumors were treated with NIR laser the next day, and tumor growth was monitor in the next 10 days before the mice were sacrificed. A single treatment of thermal ablation from both free HAuNS and pSi/HAuNS significantly inhibited tumor growth (Fig. 4). However, the pSi/HAuNS-treated mice did not have much tumor growth, while the tumor weight in the free HAuNS group more than doubled during the same period of time. In the pSi control group,

the average tumor weight almost quadrupled to 1 g/tumor. This result clearly supports the application of the pSi/HAuNS assembly in cancer therapy.

Previous studied have demonstrated the potential application of pSi as a multistage vector for the delivery of therapeutics and imaging agents [32, 33, 36]. Due to the nature of the size and porosity, pSi can be used as a cargo to deliver a large quantity of therapeutic agents, and can achieve tumoritropic accumulation independent of the EPR effect. In this study, pSi is used not only for enhanced tumor localization, but also as an essential part of the therapeutic complex for the enhancement of thermal ablation, making it a part of therapeutic mechanism. We have analyzed kinetics of heat generation by HAuNS with respect to heat exchange. Theoretical models of gold nanoparticle suspensions have been developed [37, 38], where the energy balance was governed by laser induced heat through electron-phonon relaxations on HAuNS surfaces and heat dissipation. The temperature profile generated by laser was derived by introducing the rate of energy adsorption, *A[K/s]*, and the rate of heat loss, *B[1/s]* [37]:

$$T(t)=T_0+\frac{A}{B}(1-\exp(-Bt)) \quad (1)$$

We have fitted Equation (1) to temperature profiles in Figure 2, where A = 4.17 K/s and B = 0.36 s^{-1} for HAuNS and A = 12.26 K/s and B = 0.56 s^{-1} for pSi/HAuNS. The rate of heat generations was 3 times as high for pSi/HAuNS as for free HAuNS. We had anticipated that both HAuNS and pSi/HAuNS would have similar heat loss rates, since the only difference was the inclusion of pSi in the nanoassembly. Interestingly, the heat dissipation rate was also higher for the pSi/HAuNS nanoassembly. Thus, the model in Equation (1) that was validated for colloidal gold could not explain the pSi/HAuNS temperature increase curve using the same heat loss rates. This suggests that thermal equilibrium of pSi/HAuNS is defined by different thermal properties of the system.

The clear difference between HAuNS and pSi/HAuNS was the distribution of the gold nanoparticles, which is summarized in Figure 5. Based on the amount of HAuNS and pSi used in this study, we concluded that the average gold inter-particle distance in colloid HAuNS was 1.7 μm, and free pSi particles were separated by 11 μm. In the pSi/HAuNS nanoassembly, however, HAuNS were fixed within pSi with a domain of less than 1 μm (Fig. 1). It has been reported that surface plasmons penetrate dielectric media up to hundreds of nanometers away from metal surface [39, 40], and that specific orientation of HAuNS can transfer energy over hundreds of nanometers [41]. Thus, HAuNS particles within the nanoassembly should become electromagnetically coupled mostly through dipole-dipole interactions [42], and can function as waveguide-like structures that increase energy transfer and heat production as illustrated in Figure 5. To support our finding, increased heat production in HAuNS structures through varying the angle of incident photon beam has already been observed [43]. Furthermore, bringing HAuNS closer to clusters can cause a red shift of surface polaron resonance [44] which could be over 100 nm [40]. The peak around 950 nm found in pSi/HAuNS, which was not observed in free HAuNS suspension, indicates a red shift of 200 nm. The increased wavelength in the NIR region could be used for deeper penetration into tissues, where HAuNS are arranged in a collective nanoscale structure. Potentially, enhanced heating effect can be supplemented also by scattering that increases light path.

Since convective flows inside pSi are negligible, thermal diffusion is the most important aspect. Characteristic thermal diffusion lengths of water, expressed as $L_T=\sqrt{4Dt}$ over given time t and the thermal diffusivity D = 1.4×10^{-3} cm^2/s, are 0.7 μm over 1 μs and 23.4

μm over 1 ms. Therefore, using sub-microsecond range NIR pulses, thermal expansion domains around individual HAuNS will start to overlap, while NIR pulses over 1 μs will make pSi/HAuNS a continuous thermally excited domain (thermal spot-source). Silicon has almost six times as high thermal diffusivity as water. At 80% porosity in pSi, the effective thermal diffusivity is 3.3×10^{-3} cm^2/s. It has already been shown that thermal dissipation of gold nanoparticles can be increased by wrapping gold core with silica shell [45]. So, L_T of pSi increases by almost 50% that makes heat dissipation even more efficient within premises of pSi, suggesting that induced photothermal effects can be enhanced by thermal properties of the HAuNS organizing materials.

Our results have clearly shown the superior photothermal ablation effect from pSi/HAuNS. We have demonstrated that pSi/HAuNS nanoassembly is much more efficient at heat generation than free gold nanoparticles. Moreover, the nanoassembly offers benefits of red shift to access deeper tissues and more efficient energy-to-heat conversion. These properties are enabled through exploiting nanoscale organization features of HAuNS and are demonstrated for the first time with therapeutic purposes.

Experimental Section

Fabrication of discoidal pSi particles and surface chemical modification

Discoidal pSi particles were fabricated as previously described with modifications [36]. The dried particles were then treated with piranha solution to obtain oxidized negatively charged silicon particles, and modified with 2% (v/v) 3-aminopropyltriethoxysilane (APTES) (Sigma-Aldrich, St. Louis, MO) for 24–36 hours at 55C to obtain positively charged particles for loading of nanoparticles. HAuNS synthesis was reported previously [34, 35]. HAuNS was loaded into pSi by a combination of capillary force and surface charges.

Photothermal effect in aqueous solution

The GCSLX-05-1600m-1 fiber-coupled diode laser (DHC, China Daheng Group, Beijing, China) with a center wavelength of 808 ± 10 nm was powered by a DH 1715A-5 dual-regulated power supply. A 5 m, 600-μm core BioTex LCM-001 optical fiber (BioTex Inc., Houston, TX) was used to transfer laser power from the laser unit to the target. The end of the optical fiber was attached to a retort stand using a movable clamp and positioned directly above the sample cell. For measurement of temperature changes, NIR laser light was delivered through a quartz cuvette containing pSi, HAuNS, or pSi/HAuNS (100 μL). A thermocouple was inserted into the solution perpendicular to the path of the laser light. The temperature was measured over 10 min.

Photothermal cytotoxicity in vitro

Cancer cells were seeded into a 96-well plate at a density of 10,000 cells/well. Free HAuNS or pSi/HAuNS were added into cell culture 5 hrs later when cells were attached to the plate. Cells were washed three times with serum-free media the next day, and were irradiated with NIR at an output power of 2 watts for 2 min (for SK-BR-3 cells), or 3 min (for MDA-MB-231 and 4T1 cells). Cells were washed three times with Hank's balanced salt solution 24 hr after laser treatment, and stained with the Live/Dead Viability/Cytotoxicity kit from Invitrogen according to the manufacturer suggested protocol. Live cells were stained with calcein AM and dead cells were stained with ethidium homodimer. Cells were examined using an Olympus Fluoview FV1000 confocal laser scanning microscope (FV1-ASW) equipped with filter sets specific for excitation/emission wavelengths at 494/517 nm for live cells (stained in green) and 528/617 nm for dead cells (stained in red).

Photothermal therapy of mammary tumor in nude mice

Six-week old nude mice were inoculated with 4T1 cells in the mammary gland fat pad. When tumors reached 150–200 mm^3 sizes, the mice were administered with PBS, pSi, HAuNS, or pSi/HAuNS by intra-tumor injection. Each mouse in the treatment group received 3×10^8 pSi containing 1×10^{11} HAuNS in 25 μL PBS. In the control groups, each mouse received 25 μL PBS, 3×10^8 empty pSi, or 1×10^{11} free HAuNS. The mice were treated with NIR at 0.5 watt for 3 min per tumor, and tumor growth was monitored in the next two weeks. All animals were sacrificed when tumor sizes in the PBS control group passed 1,000 mm^3.

Supplementary Material

Refer to Web version on PubMed Central for supplementary material.

Acknowledgments

The authors acknowledge financial supports from the following sources: Department of Defense grant DODW81XWH-09-1-0212, National Institute of Health grants NIH RO1CA128797, NIH – R33 CA122864, and NIH U54CA143837.

Abbreviations

pSi	porous silicon
HAuNS	hollow gold nanoshells
AuNP	gold nanoparticles
pSi/HAuNS	hollow gold nanoshell in porous silicon
NIR	near infrared

References

1. Jemal A, Siegel R, Xu J, Ward E. CA Cancer J Clin. 2010; 60:277. [PubMed: 20610543]
2. Parsons DW, Jones S, Zhang X, Lin JC, Leary RJ, Angenendt P, Mankoo P, Carter H, Siu IM, Gallia GL, Olivi A, McLendon R, Rasheed BA, Keir S, Nikolskaya T, Nikolsky Y, Busam DA, Tekleab H, Diaz LA Jr, Hartigan J, Smith DR, Strausberg RL, Marie SK, Shinjo SM, Yan H, Riggins GJ, Bigner DD, Karchin R, Papadopoulos N, Parmigiani G, Vogelstein B, Velculescu VE, Kinzler KW. Science. 2008; 321:1807. [PubMed: 18772396]
3. Jones S, Zhang X, Parsons DW, Lin JC, Leary RJ, Angenendt P, Mankoo P, Carter H, Kamiyama H, Jimeno A, Hong SM, Fu B, Lin MT, Calhoun ES, Kamiyama M, Walter K, Nikolskaya T, Nikolsky Y, Hartigan J, Smith DR, Hidalgo M, Leach SD, Klein AP, Jaffee EM, Goggins M, Maitra A, Iacobuzio-Donahue C, Eshleman JR, Kern SE, Hruban RH, Karchin R, Papadopoulos N, Parmigiani G, Vogelstein B, Velculescu VE, Kinzler KW. Science. 2008; 321:1801. [PubMed: 18772397]
4. Wood LD, Parsons DW, Jones S, Lin J, Sjoblom T, Leary RJ, Shen D, Boca SM, Barber T, Ptak J, Silliman N, Szabo S, Dezso Z, Ustyanksky V, Nikolskaya T, Nikolsky Y, Karchin R, Wilson PA, Kaminker JS, Zhang Z, Croshaw R, Willis J, Dawson D, Shipitsin M, Willson JK, Sukumar S, Polyak K, Park BH, Pethiyagoda CL, Pant PV, Ballinger DG, Sparks AB, Hartigan J, Smith DR, Suh E, Papadopoulos N, Buckhaults P, Markowitz SD, Parmigiani G, Kinzler KW, Velculescu VE, Vogelstein B. Science. 2007; 318:1108. [PubMed: 17932254]
5. Lynch TJ, Bell DW, Sordella R, Gurubhagavatula S, Okimoto RA, Brannigan BW, Harris PL, Haserlat SM, Supko JG, Haluska FG, Louis DN, Christiani DC, Settleman J, Haber DA. N Engl J Med. 2004; 350:2129. [PubMed: 15118073]

6. Paez JG, Janne PA, Lee JC, Tracy S, Greulich H, Gabriel S, Herman P, Kaye FJ, Lindeman N, Boggon TJ, Naoki K, Sasaki H, Fujii Y, Eck MJ, Sellers WR, Johnson BE, Meyerson M. Science. 2004; 304:1497. [PubMed: 15118125]
7. Balak MN, Gong Y, Riely GJ, Somwar R, Li AR, Zakowski MF, Chiang A, Yang G, Ouerfelli O, Kris MG, Ladanyi M, Miller VA, Pao W. Clin Cancer Res. 2006; 12:6494. [PubMed: 17085664]
8. Kobayashi S, Boggon TJ, Dayaram T, Janne PA, Kocher O, Meyerson M, Johnson BE, Eck MJ, Tenen DG, Halmos B. N Engl J Med. 2005; 352:786. [PubMed: 15728811]
9. Pao W, Wang TY, Riely GJ, Miller VA, Pan Q, Ladanyi M, Zakowski MF, Heelan RT, Kris MG, Varmus HE. PLoS Med. 2005; 2:e17. [PubMed: 15696205]
10. Eberhard DA, Johnson BE, Amler LC, Goddard AD, Heldens SL, Herbst RS, Ince WL, Janne PA, Januario T, Johnson DH, Klein P, Miller VA, Ostland MA, Ramies DA, Sebisanovic D, Stinson JA, Zhang YR, Seshagiri S, Hillan KJ. J Clin Oncol. 2005; 23:5900. [PubMed: 16043828]
11. Engelman JA, Zejnullahu K, Mitsudomi T, Song Y, Hyland C, Park JO, Lindeman N, Gale CM, Zhao X, Christensen J, Kosaka T, Holmes AJ, Rogers AM, Cappuzzo F, Mok T, Lee C, Johnson BE, Cantley LC, Janne PA. Science. 2007; 316:1039. [PubMed: 17463250]
12. Bean J, Brennan C, Shih JY, Riely G, Viale A, Wang L, Chitale D, Motoi N, Szoke J, Broderick S, Balak M, Chang WC, Yu CJ, Gazdar A, Pass H, Rusch V, Gerald W, Huang SF, Yang PC, Miller V, Ladanyi M, Yang CH, Pao W. Proc Natl Acad Sci U S A. 2007; 104:20932. [PubMed: 18093943]
13. Ferrari M. Nat Rev Cancer. 2005; 5:161. [PubMed: 15738981]
14. Rahman A, Treat J, Roh JK, Potkul LA, Alvord WG, Forst D, Woolley PV. J Clin Oncol. 1990; 8:1093. [PubMed: 2348224]
15. Treat J, Greenspan A, Forst D, Sanchez JA, Ferrans VJ, Potkul LA, Woolley PV, Rahman A. J Natl Cancer Inst. 1990; 82:1706. [PubMed: 2231759]
16. Ibrahim NK, Samuels B, Page R, Doval D, Patel KM, Rao SC, Nair MK, Bhar P, Desai N, Hortobagyi GN. J Clin Oncol. 2005; 23:6019. [PubMed: 16135470]
17. Gradishar WJ, Tjulandin S, Davidson N, Shaw H, Desai N, Bhar P, Hawkins M, O'Shaughnessy J. J Clin Oncol. 2005; 23:7794. [PubMed: 16172456]
18. Hirsch LR, Stafford RJ, Bankson JA, Sershen SR, Rivera B, Price RE, Hazle JD, Halas NJ, West JL. Proc Natl Acad Sci U S A. 2003; 100:13549. [PubMed: 14597719]
19. Glazer ES, Curley SA. Cancer. 2010; 116:3285. [PubMed: 20564640]
20. O'Neal DP, Hirsch LR, Halas NJ, Payne JD, West JL. Cancer Lett. 2004; 209:171. [PubMed: 15159019]
21. Schwartz JA, Shetty AM, Price RE, Stafford RJ, Wang JC, Uthamanthil RK, Pham K, McNichols RJ, Coleman CL, Payne JD. Cancer Res. 2009; 69:1659. [PubMed: 19208847]
22. Dickerson EB, Dreaden EC, Huang X, El-Sayed IH, Chu H, Pushpanketh S, McDonald JF, El-Sayed MA. Cancer Lett. 2008; 269:57. [PubMed: 18541363]
23. Kennedy LC, Bickford LR, Lewinski NA, Coughlin AJ, Hu Y, Day ES, West JL, Drezek RA. Small. 2011; 7:169. [PubMed: 21213377]
24. Maeda H. Adv Enzyme Regul. 2001; 41:189. [PubMed: 11384745]
25. Puvanakrishnan P, Park J, Diagaradjane P, Schwartz JA, Coleman CL, Gill-Sharp KL, Sang KL, Payne JD, Krishnan S, Tunnell JW. J Biomed Opt. 2009; 14:024044. [PubMed: 19405772]
26. Perrault SD, Walkey C, Jennings T, Fischer HC, Chan WC. Nano Lett. 2009; 9:1909. [PubMed: 19344179]
27. Kim B, Han G, Toley BJ, Kim CK, Rotello VM, Forbes NS. Nat Nanotechnol. 2010; 5:465. [PubMed: 20383126]
28. Tasciotti E, Liu X, Bhavane R, Plant K, Leonard AD, Price BK, Cheng MM, Decuzzi P, Tour JM, Robertson F, Ferrari M. Nat Nanotechnol. 2008; 3:151. [PubMed: 18654487]
29. Ferrari M. Trends Biotechnol. 2010; 28:181. [PubMed: 20079548]
30. Decuzzi P, Ferrari M. Biomaterials. 2008; 29:377. [PubMed: 17936897]
31. Decuzzi P, Godin B, Tanaka T, Lee SY, Chiappini C, Liu X, Ferrari M. J Control Release. 2010; 141:320. [PubMed: 19874859]

32. Tanaka T, Mangala LS, Vivas-Mejia PE, Nieves-Alicea R, Mann AP, Mora E, Han HD, Shahzad MM, Liu X, Bhavane R, Gu J, Fakhoury JR, Chiappini C, Lu C, Matsuo K, Godin B, Stone RL, Nick AM, Lopez-Berestein G, Sood AK, Ferrari M. Cancer Res. 2010; 70:3687. [PubMed: 20430760]
33. Ferrari M. Nat Rev Clin Oncol. 2010; 7:485. [PubMed: 20798696]
34. You J, Zhang G, Li C. ACS Nano. 2010; 4:1033. [PubMed: 20121065]
35. Lu W, Xiong C, Zhang G, Huang Q, Zhang R, Zhang JZ, Li C. Clin Cancer Res. 2009; 15:876. [PubMed: 19188158]
36. Ananta JS, Godin B, Sethi R, Moriggi L, Liu X, Serda RE, Krishnamurthy R, Muthupillai R, Bolskar RD, Helm L, Ferrari M, Wilson LJ, Decuzzi P. Nat Nanotechnol. 2010; 5:815. [PubMed: 20972435]
37. Richardson HH, Carlson MT, Tandler PJ, Hernandez P, Govorov AO. Nano Lett. 2009; 9:1139. [PubMed: 19193041]
38. Roper DK, Ahn W, Hoepfner M. The Journal of Physical Chemistry C. 2007; 111:3636.
39. Huang CJ, Dostalek J, Knoll W. Biosens Bioelectron. 2010; 26:1425. [PubMed: 20727729]
40. Jensen T, Kelly L, Lazarides A, Schatz GC. J Cluster Sci. 1999; 10:295.
41. Maier SA, Kik PG, Atwater HA, Meltzer S, Harel E, Koel BE, Requicha AAG. Nat Mater. 2003; 2:229. [PubMed: 12690394]
42. Rechberger W, Hohenau A, Leitner A, Krenn J, Lamprecht B, Aussenegg F. Opt Commun. 2003; 220:137.
43. Govorov AO, Zhang W, Skeini T, Richardson H, Lee J, Kotov NA. Nanoscale Research Letters. 2006; 1:84.
44. Hövel H, Fritz S, Hilger A, Kreibig U, Vollmer M. Physical Review B. 1993; 48:18178.
45. Hu M, Wang X, Hartland G, Salgueiriño-Maceira V, Liz-Marzán L. Chem Phys Lett. 2003; 372:767.

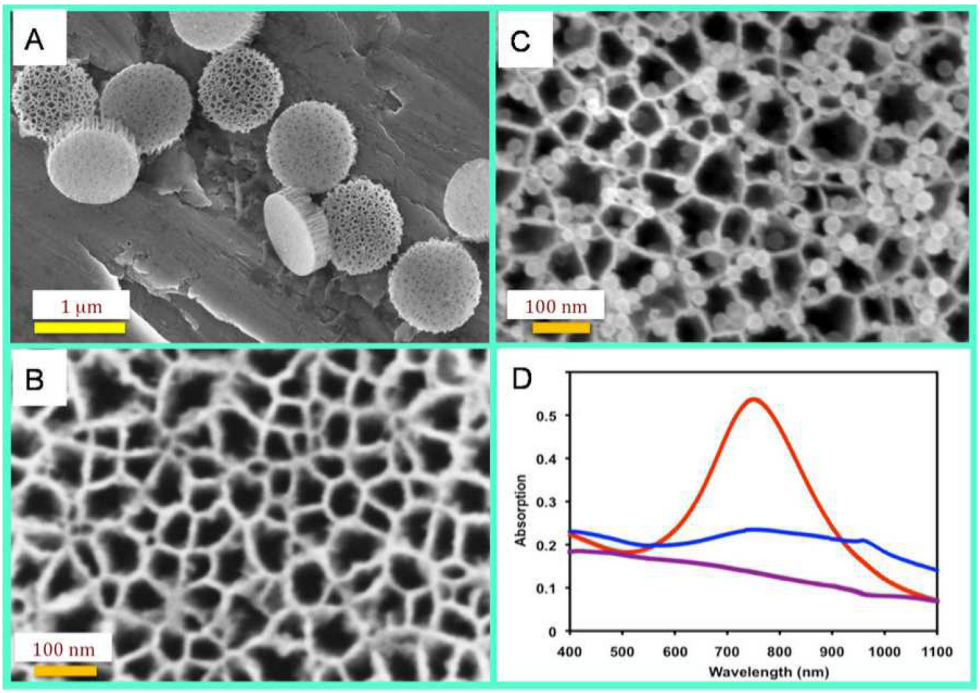

Figure 1.

Scanning electron microscope (SEM) images of empty pSi and pSi/HAuNS. The SEM imaging of particles was performed using a ZEISS NEON 40 scanning electron microscope. To prepare SEM sample, a drop of IPA particle suspension was directly placed on a clean aluminum SEM sample stub and dried. The samples were loaded in SEM chamber, and SEM images were measured at 5kV and 3–5 mm working distance using an in-lens detector. (A & B): SEM images of monodispersed 1000 nm × 400 nm discoidal pSi particles with 60 nm mean pore size. (C): SEM image of silicon particles loaded with HAuNS. (D): Absorption spectra of pSi (purple), HAuNS (red), and pSi/HAuNS (blue).

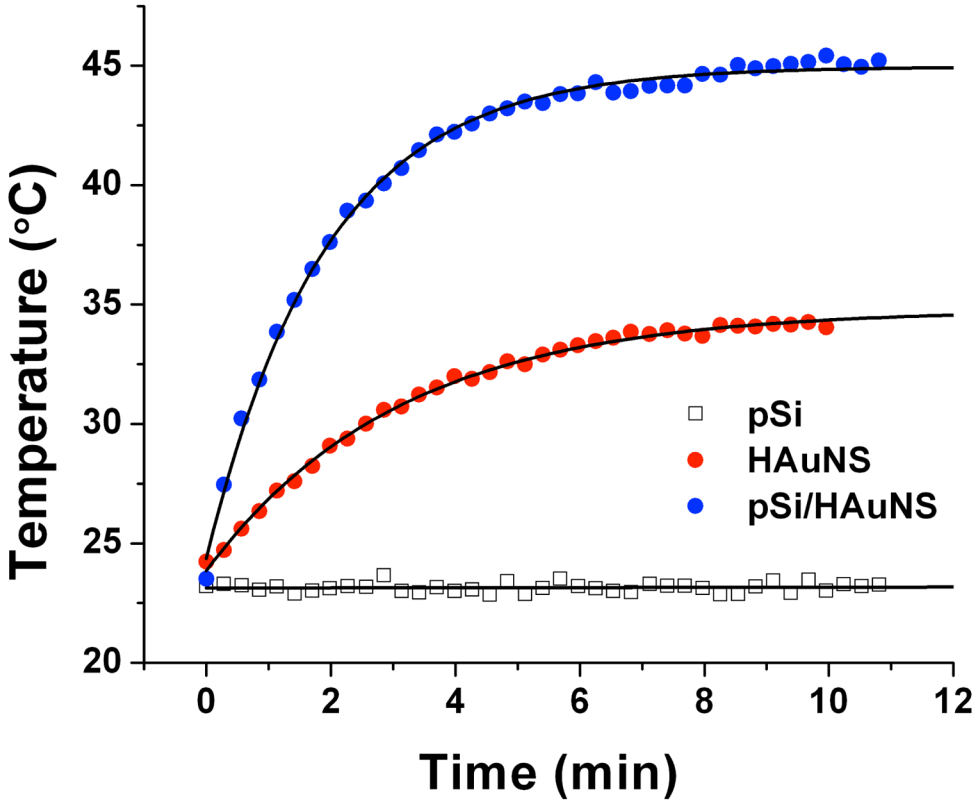

Figure 2.

Heat generation kinetics from free HAuNS and pSi/HAuNS. Temperature change was measured over a period of 10 min of exposure to NIR with a wavelength of 808 nm and an output power of 0.5 w. Same amount of HAuNS particles were used in the samples of free HAuNS and pSi/HAuNS. Equal amount of unloaded pSi particles as in pSi/HAuNS were used as a control. Experimental data were shown with best exponential fit.

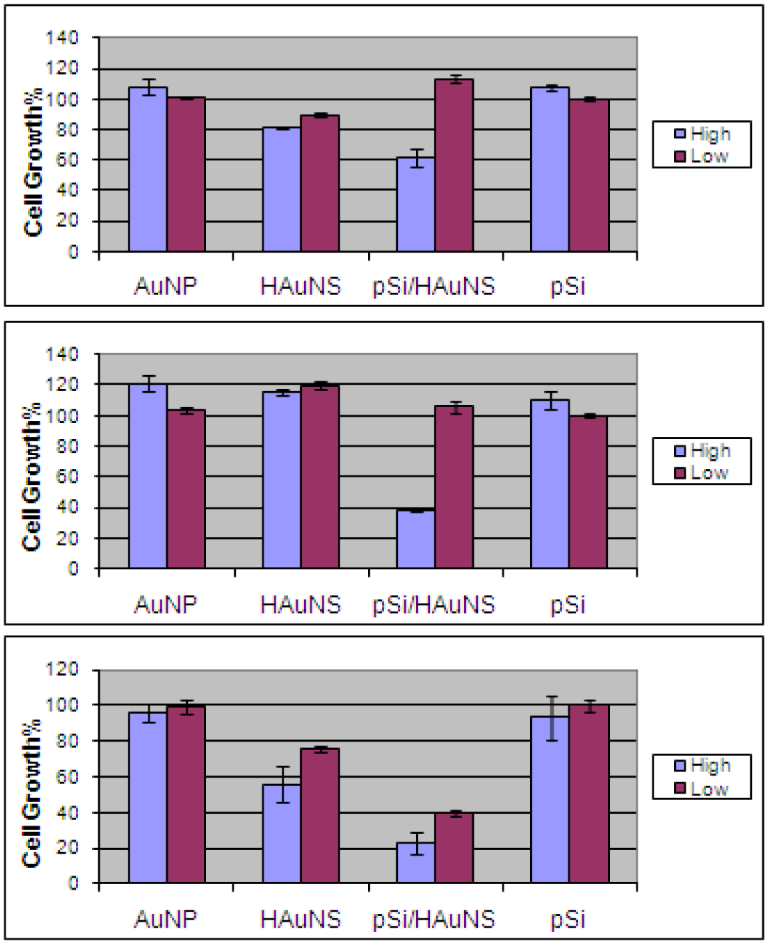

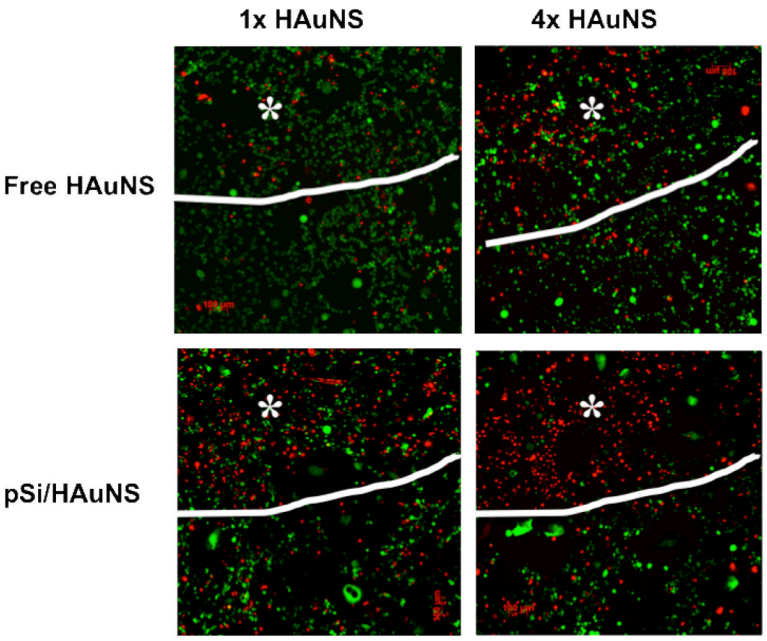

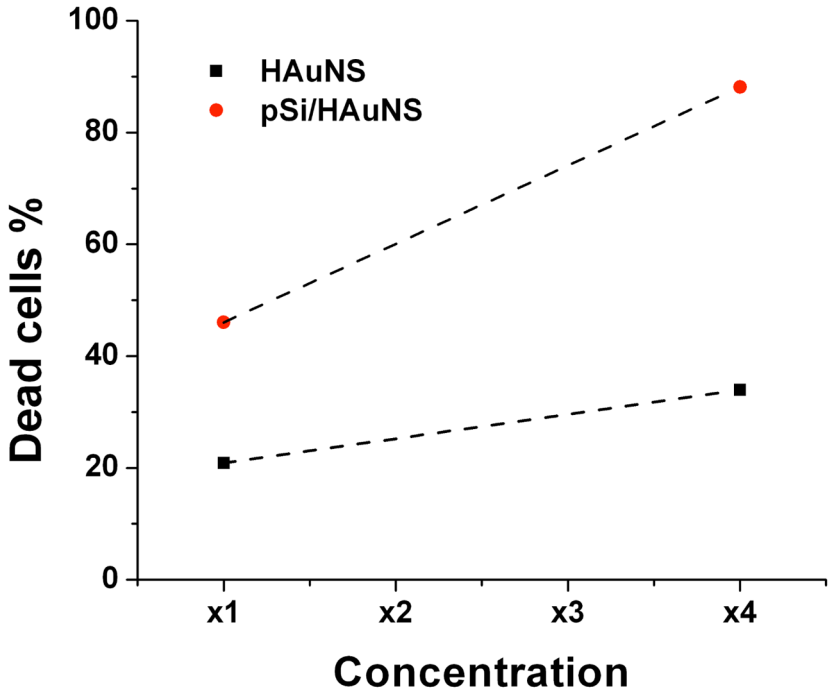

Figure 3.

Photothermal effect on cancer cell growth *in vitro* and *in vivo*. (A). Cell survival as a function of HAuNS concentration. Cancer cells were incubated with a high dose (2×10^{10}/well, in blue) and a low dose (2×10^{9}/well, in purple) of free AuNP, free HAuNS, or pSi/HAuNS, and treated with NIR. Cell survival was measured by the MTT assay. Percentage of cell growth was calculated by comparing the growth of treated cells to untreated control cells. Upper panel: MDA-MB-231 cells; middle panel: SK-BR-3 cells; bottom panel: 4T1 cells.

(B). Cell viability staining after NIR treatment of MDA-MB-231 cells incubated with free HAuNS or pSi/HAuNS. MDA-MB-231 cells were incubated with a low-dose (1X) or a high dose (4X) free HAuNS or pSi/HAuNS, and treated with NIR. Live cells were stained green with calcein AM, and dead cells were stained red with EthD-1. The boundary of NIR laser beam was marked with a white line in each well, and the area hit by laser was marked with an asterisk.

(C). Analysis of cell staining result. Percentage of dead cells in each well was normalized with untreated control cells.

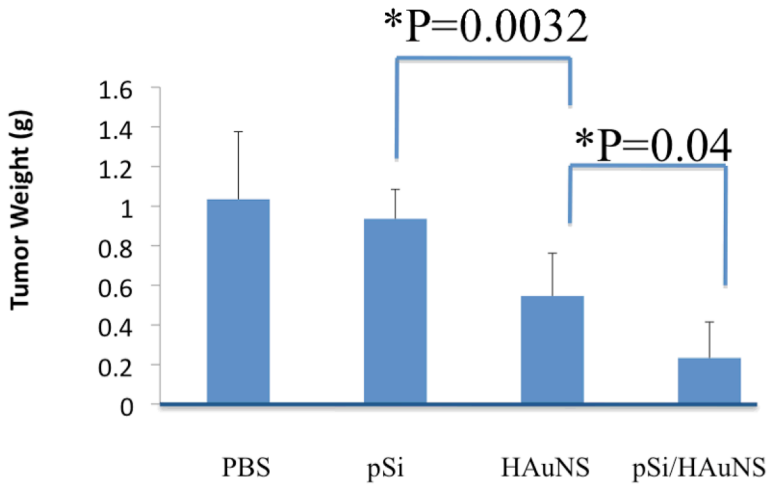

Figure 4.

Photothermal therapy of murine 4T1 tumor. Mice were inoculated with 4T1 tumor cells, and divided into 4 treatment groups (n = 8). When tumors reached an average size of 150–200 cm^3, the tumor mice were administrated with free HAuNS or the same amount of HAuNS in pSi nanoassembly by intra-tumor injection, and treated with NIR. The PBS and pSi groups served as controls. The result was a summary of tumor weight 10 days after treatment.

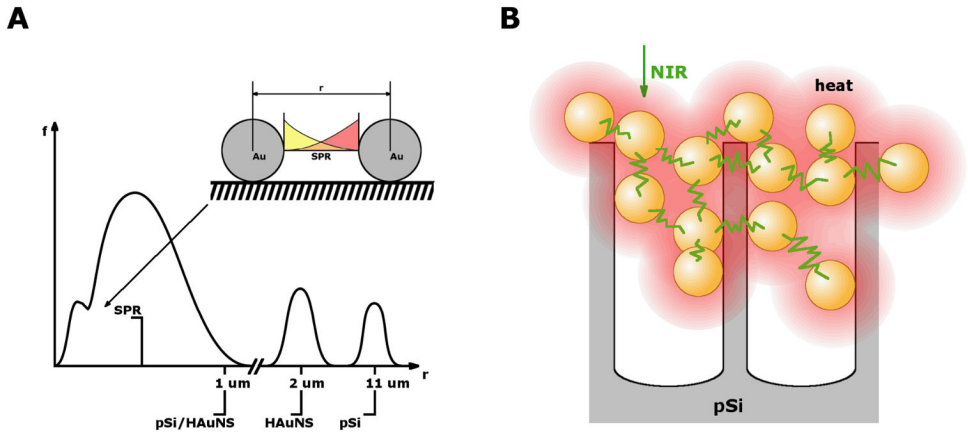

Figure 5.

Potential mechanism of increased thermal efficiency from pSi/HAuNS. A) Characteristic interparticle distances in our experiments for pSi, HAuNS and pSi/HAuNS. HAuNS and surface polaron interaction distances overlap enabling HAuNS electromagnetic coupling within pSi, which is not possible for free HAuNS. B) Proposed schematics of collective electromagnetic coupling of HAuNS in pSi leading to coherent thermal domain.